

Testing the Technicolor Interpretation of CDF's Dijet Excess at the LHC

Estia Eichten^{1*}, Kenneth Lane^{2†}, Adam Martin^{1‡} and Eric Pilon^{3§}

¹Theoretical Physics Group, Fermi National Accelerator Laboratory
P.O. Box 500, Batavia, Illinois 60510

²Department of Physics, Boston University
590 Commonwealth Avenue, Boston, Massachusetts 02215

³Laboratoire d'Annecy-le-Vieux de Physique Théorique
UMR5108, Université de Savoie, CNRS
B.P. 110, F-74941, Annecy-le-Vieux Cedex, France

January 24, 2012

Abstract

Under the assumption that the dijet excess seen by the CDF Collaboration near 150 GeV in Wjj production is due to the lightest technipion of the low-scale technicolor process $\rho_T \rightarrow W\pi_T$, we study its observability in LHC detectors with 1–20 fb⁻¹ of data. We describe interesting new kinematic tests that can provide independent confirmation of this LSTC hypothesis. We find that cuts similar to those employed by CDF, and recently by ATLAS, cannot confirm the dijet signal. We propose cuts tailored to the LSTC hypothesis and its backgrounds at the LHC that may reveal $\rho_T \rightarrow \ell\nu jj$. Observation of the isospin-related channel $\rho_T^\pm \rightarrow Z\pi_T^\pm \rightarrow \ell^+\ell^-jj$ and of $\rho_T^\pm \rightarrow WZ$ in the $\ell^+\ell^-\ell^\pm\nu_\ell$ and $\ell^+\ell^-jj$ modes will be important confirmations of the LSTC interpretation of the CDF signal. The $Z\pi_T$ channel is experimentally cleaner than $W\pi_T$ and its rate is known from $W\pi_T$ by phase space. It can be discovered or excluded with the collider data expected in 2012. The $WZ \rightarrow 3\ell\nu$ channel is cleanest of all and its rate is determined from $W\pi_T$ and the LSTC parameter $\sin\chi$. This channel and $WZ \rightarrow \ell^+\ell^-jj$ are discussed as a function of $\sin\chi$.

*eichten@fnal.gov

†lane@physics.bu.edu

‡aomartin@fnal.gov

§pilon@lapp.in2p3.fr

1. Introduction

The CDF Collaboration has reported evidence for a resonance near 150 GeV in the dijet-mass spectrum, M_{jj} , of Wjj production. This is based on an integrated luminosity of 4.3 fb^{-1} [1] and updated with a total data sample of 7.3 fb^{-1} [2]. In Ref. [2], the resonant dijet excess has a significance of 4.1σ . The DØ Collaboration, on the other hand, published a search for this resonance based on 4.3 fb^{-1} that found no significant excess. Based on a W +Higgs boson production model, DØ reported a cross section for a potential signal of $0.82^{+0.83}_{-0.82} \text{ pb}$ and a 95% confidence level upper limit of 1.9 pb [3]. Analyzing its data with the same production model, CDF reported a signal rate of $3.0 \pm 0.7 \text{ pb}$ and a discrepancy between the two experiments of 2.5σ [4]. This discrepancy remains. The purpose of this paper is to urge that the LHC experiments, ATLAS and CMS, mount searches to test for the CDF dijet excess in the Wjj and closely related channels. We do this in the context low-scale technicolor (LSTC), interpreting CDF’s dijet excess as the lightest technipion $\pi_T^{\pm,0}$ of this scenario, produced in association with W^\pm in the decay $\rho_T^{\pm,0} \rightarrow W\pi_T$ [5]. The related channels supporting this interpretation are $\rho_T^\pm \rightarrow Z\pi_T^\pm$ and $W^\pm Z$. They require the fewest additional LSTC model assumptions to determine LHC production rates. We assume $\sqrt{s} = 7 \text{ TeV}$ and consider $\int \mathcal{L} dt = 1\text{--}20 \text{ fb}^{-1}$, an amount of data expected in 2012.¹

Low-scale technicolor (LSTC) is a phenomenology based on walking technicolor [7, 8, 9, 10]. The gauge coupling α_{TC} must run very slowly for 100s of TeV above the TC scale $\Lambda_{TC} \sim$ several 100 GeV so that extended technicolor (ETC) can generate sizable quark and lepton masses while suppressing flavor-changing neutral current interactions [11]. This may be achieved, e.g., with technifermions belonging to higher-dimensional representations of the TC gauge group. The constraints of Ref. [11] on the number of ETC-fermion representations then imply that there will be technifermions in the fundamental TC representation as well. They are expected to condense at an appreciably lower energy scale than those belonging to the higher-dimensional representations and, thus, their technipions’ decay constant $F_1^2 \ll F_\pi^2 = (246 \text{ GeV})^2$ [12]. Meson bound states of these technifermions will have a quarkonium-like spectrum with masses well below a TeV — greater than the previous Tevatron limit $M_{\rho_T} \gtrsim 250 \text{ GeV}$ [13, 14] and probably less than 600–700 GeV, a scale at which we believe the notion of “low-scale” TC ceases to make sense. The most accessible states are the lightest technivectors, $V_T = \rho_T(I^G J^{PC} = 1^+ 1^{--})$, $\omega_T(0^- 1^{--})$ and $a_T(1^- 1^{++})$. Through their mixing with the electroweak bosons, they are readily produced as s -channel resonances via the Drell-Yan process in colliders. Technipions $\pi_T(1^- 0^{-+})$ are accessed in V_T decays. A central assumption of LSTC is that these lightest technihadrons may be treated in isolation, without significant mixing or other interference from higher-mass states. Also, we expect

¹A preliminary version of this paper was circulated as Ref. [6], assuming $\int \mathcal{L} dt = 1\text{--}5 \text{ fb}^{-1}$. The simulations we present here for various fixed luminosities may be applied to different ones by scaling the event rates. The question of raising the LHC collision energy to 8 TeV in 2012 is under consideration. This probably will not be advantageous for the LSTC signals discussed here and elsewhere because backgrounds, especially gluon-induced ones, grow faster with energy than do the signals.

that (1) the lightest technifermions are $SU(3)$ -color singlets, (2) isospin violation is small for V_T and π_T , (3) $M_{\omega_T} \cong M_{\rho_T}$, and (4) M_{a_T} is not far above M_{ρ_T} . This last assumption is made to keep the low-scale TC contribution to the S -parameter small. An extensive discussion of LSTC, including these points and precision electroweak constraints, is given in Ref. [15].

Walking technicolor has another important consequence: it enhances M_{π_T} relative to M_{ρ_T} so that the all- π_T decay channels of the V_T are likely to be closed [12]. Principal V_T -decay modes are $W\pi_T$, $Z\pi_T$, $\gamma\pi_T$, a pair of EW bosons (which can include one photon), and fermion-antifermion pairs [16, 17, 15]. If allowed by isospin, parity and angular momentum, V_T decays to one or more weak bosons involve longitudinally-polarized W_L/Z_L , the technipions absorbed via the Higgs mechanism. These nominally strong decays are suppressed by powers of $\sin\chi = F_1/F_\pi \ll 1$. This is an important parameter in LSTC. It is a mixing factor that measures the amount that the lowest-scale technipion is the mass eigenstate π_T ($\cos\chi$) and the amount that it is W_L/Z_L ($\sin\chi$). Thus, each replacement of a mass-eigenstate π_T by W_L/Z_L in a V_T decay amplitude costs a factor of $\tan\chi$. Decays to transversely-polarized γ, W_\perp, Z_\perp are suppressed by g, g' . Thus, the V_T are *very* narrow, $\Gamma(\rho_T) \lesssim 1 \text{ GeV}$ and $\Gamma(\omega_T, a_T) \lesssim 0.1 \text{ GeV}$ for the masses considered here. These decays have striking signatures, visible above backgrounds within a limited mass range at the Tevatron and probably up to 600–700 GeV at the LHC [18, 19].

In Ref. [5] we proposed that CDF's dijet excess is due to resonant production of $W\pi_T$ with $M_{\pi_T} = 160 \text{ GeV}$. We took $M_{\rho_T} = 290 \text{ GeV}$ and $M_{a_T} = 1.1M_{\rho_T} = 320 \text{ GeV}$. Then, about 75% of the $W\pi_T$ rate at the Tevatron is due to $\rho_T \rightarrow W\pi_T$ and, of this, most of the W 's are longitudinally polarized.² The remainder is dominated by a_T production. Its decay, and a small fraction of the ρ_T 's, involve W_\perp production, which is generated by dimension-five operators [15]. These operators are suppressed by mass parameters $M_{V,A}$ that we take equal to M_{ρ_T} . The other LSTC parameters relevant to $W\pi_T$ production are $g_{\rho_T\pi_T\pi_T}$ and $\sin\chi$. The $\rho_T \rightarrow \pi_T\pi_T$ coupling $g_{\rho_T\pi_T\pi_T}$ is the same for all ρ_T decays considered here and it is simply scaled from QCD; its PYTHIA default value is $\alpha_{\rho_T} = g_{\rho_T\pi_T\pi_T}^2/4\pi = 2.16(3/N_{TC})$ with $N_{TC} = 4$. We use $\sin\chi = 1/3$. Using the LSTC model implemented in PYTHIA [16, 17, 20], we found $\sigma(\bar{p}p \rightarrow \rho_T \rightarrow W\pi_T \rightarrow Wjj) = 2.2 \text{ pb}$ (480 fb after $W \rightarrow e\nu, \mu\nu$).³ Using CDF's cuts, we closely matched its M_{jj} distribution for signal and background. Motivated by the peculiar kinematics of ρ_T production at the Tevatron and $\rho_T \rightarrow W\pi_T$ decay, we also suggested cuts intended to enhance the π_T signal's significance and to make $\rho_T \rightarrow Wjj$ visible. Several distributions of data in the excess region $115 \text{ GeV} < M_{jj} < 175 \text{ GeV}$ published by CDF [2] — notably $M_{Wjj}, p_T(jj), \Delta\phi$ and $\Delta R = \sqrt{(\Delta\eta)^2 + (\Delta\phi)^2}$ — fit the expectations of the LSTC model very well. The background-subtracted ΔR distribution, in particular, has a behavior which, we believe, furnishes strong support for our dijet production mechanism.

The purpose of this paper is to propose and study ways to test for the CDF signal at the LHC. In Sec. 2 we review the kinematics of $\rho_T, a_T \rightarrow W\pi_T$ and $Z\pi_T$ in LSTC. We also

²About 70% of the $W\pi_T$ rate at the LHC is due to the ρ_T .

³This includes $B(\pi_T \rightarrow \bar{q}q) \simeq 90\%$ in the default PYTHIA π_T -decay table.

present an interesting new result: the nonanalytic behavior of $d\sigma/d(\Delta R)$ and $d\sigma/d(\Delta\chi)$ at their thresholds, $(\Delta R)_{\min}$ and $(\Delta\chi)_{\min}$. Here $\Delta\chi$ is the opening angle between the π_T decay jets in the ρ_T rest frame. For massless jets, a good approximation, we find that $(\Delta R)_{\min} = (\Delta\chi)_{\min} = 2 \cos^{-1}(v)$, where $v = p_{\pi_T}/E_{\pi_T}$ is the π_T velocity in the ρ_T rest frame. This result, peculiar to production models such as LSTC in which a narrow resonance decays to another narrow resonance plus a W or Z , provides measures of v independent of p/E and, hence, valuable corroboration of this type of production. In Sec. 3 we consider the $\rho_T, a_T \rightarrow W\pi_T$ process. Its LHC cross section is 7.9 pb but, for CDF cuts, its backgrounds have increased by about a factor of ten. This makes testing for the dijet excess in this channel very challenging. We suggest cuts which enhance signal-to-background (S/B) but which will still require a very good understanding of the backgrounds in Wjj production and perhaps luminosity $\gtrsim 10 \text{ fb}^{-1}$ to observe, or exclude, this signal. In Sec. 4 we study $\rho_T^\pm, a_T^\pm \rightarrow Z\pi_T^\pm$, whose cross section is 2.3 pb at 7 TeV (155 fb after $Z \rightarrow e^+e^-, \mu^+\mu^-$). This is the isospin partner of $\rho_T^\pm, a_T^\pm \rightarrow W\pi_T^0$, so its cross section is rather confidently known. The $\ell^+\ell^-jj$ channel is free of QCD multijet and $\bar{t}t$ backgrounds and missing energy uncertainty. Reconstructing the Zjj invariant mass and other signal distributions, particularly in ΔR and $\Delta\chi$, will benefit from this. *Because of these features, we believe that the $Z\pi_T \rightarrow Zjj$ mode will be the surest test of CDF's dijet signal at the LHC.* In Sec. 5, we study $\rho_T^\pm, a_T^\pm \rightarrow WZ$. The cross section for this mode is proportional to $\tan^2 \chi$ times the $\rho_T^\pm, a_T^\pm \rightarrow W^\pm\pi_T^0$ and $Z\pi_T^\pm$ rates, but enhanced by its greater phase space. We predict $\sigma(\rho_T^\pm, a_T^\pm \rightarrow WZ) = 1.3 \text{ pb}$ for $\sin \chi = 1/3$. In the all-leptons mode (with e 's and μ 's), the rate is only 20 fb, but jet-related uncertainties are entirely absent. The $WZ \rightarrow \ell^+\ell^-jj$ mode is also an interesting target of opportunity so long as $\sin \chi \gtrsim 1/4$. The ΔR and $\Delta\chi$ distributions for $Z \rightarrow jj$ again provide support for our narrow LSTC-resonance production model. In short, one or both of the $Z\pi_T$ and WZ modes should be accessible with the $\gtrsim 20 \text{ fb}^{-1}$ expected to be in hand by the end of 2012. Finally, we present in an appendix the details of calculations in Sec. 2 regarding the nonanalytic threshold behavior of the $\Delta\chi$ and ΔR distributions.

While the simulations of the CDF signal in this paper are made in the context of low-scale technicolor, their qualitative features apply to any model in which that signal is due to $\bar{q}q$ production of a narrow resonance decaying to a W plus another narrow resonance. Several papers have appeared proposing such an s -channel mechanism [21, 22, 23, 24, 25, 26]. With similar resonance masses to our LSTC proposal, these models will have kinematic distributions like those we describe in Sec. 2. However, not all these models will have the Zjj and WZ signals of LSTC. There are also a large number of papers proposing that the CDF signal is due to production of a new particle (e.g., a leptophobic Z') that is not resonantly produced [27, 28, 29, 30, 31, 32, 33]. These “ t -channel” models will not pass our kinematic tests.

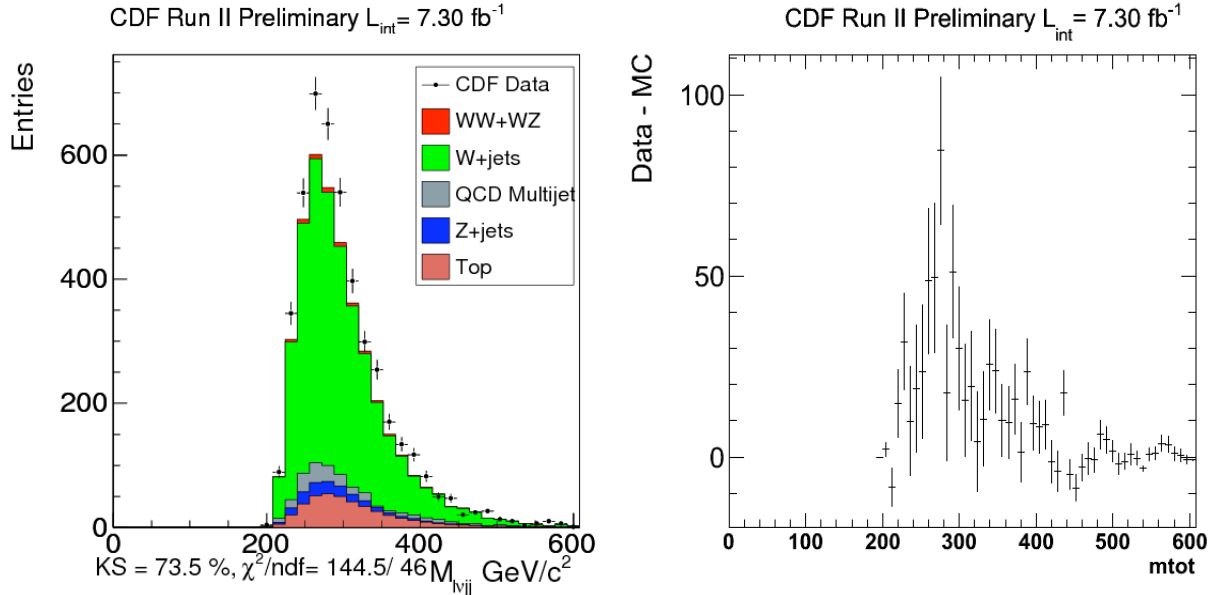


Figure 1: CDF M_{Wjj} distributions for $\int \mathcal{L} dt = 7.3 \text{ fb}^{-1}$ from the dijet signal region $115 < M_{jj} < 175 \text{ GeV}$ [2]. Left: Expected backgrounds and data; right: background subtracted data.

2. LSTC Kinematics and Threshold Nonanalyticity

The kinematics of $\rho_T \rightarrow W\pi_T$ at the Tevatron and LHC are a consequence of the basic LSTC feature that walking TC enhancements of M_{π_T} strongly suggest $M_{\rho_T} < 2M_{\pi_T}$ and, indeed, that the phase space for $\rho_T \rightarrow W\pi_T$ is quite limited [12, 34]. At the Tevatron, a 290 GeV ρ_T is produced almost at rest, with almost no p_T and very little boost along the beam direction. At the LHC, $p_T(\rho_T) \lesssim 25 \text{ GeV}$ and $\eta(\rho_T) \lesssim 2.0$. Furthermore, the π_T is emitted very slowly in the ρ_T rest frame — $v \simeq 0.4$ for our assumed masses — so that its decay jets are roughly back-to-back in the lab frame. Thus, $p_T(\pi_T) \lesssim 80 \text{ GeV}$ and the z -boost invariant quantities $\Delta\phi$ and $\Delta R = \sqrt{(\Delta\eta)^2 + (\Delta\phi)^2}$ are peaked at large values less than π .

These features of LSTC are supported by CDF's 7.3 fb^{-1} data [2]. Figures 1–4 show distributions before and after background subtraction taken from the $115 < M_{jj} < 175 \text{ GeV}$ region containing the dijet excess. The subtracted-data M_{Wjj} signal has a narrow resonant shape quite near 290 GeV. Unfortunately, the background peaks just below that mass so that one may be concerned that the subtracted data's peak is due to underestimating the background. Also, as we expect, the subtracted $p_T(jj)$ data falls off sharply above 75 GeV and the subtracted $\Delta\phi$ data is strongly peaked at large values. Again, one may worry that these are artifacts of the peaks of the M_{Wjj} background and the position of the M_{jj} excess.

The background-subtracted ΔR distribution, however, is very interesting. It is practically zero for $\Delta R < 2.25$, then rises sharply to a broad maximum before falling to zero again at $\Delta R \simeq 3.5$. This behavior, and a somewhat similar one we predict for $\Delta\chi$ are the main subject

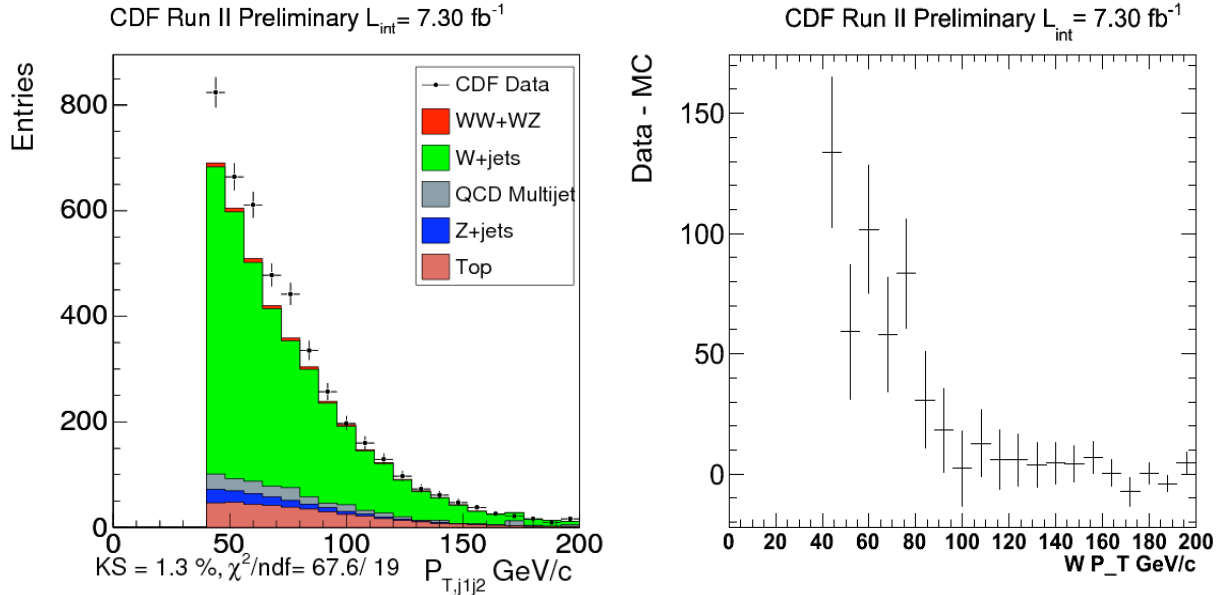


Figure 2: CDF $p_T(jj)$ distributions for $\int \mathcal{L} dt = 7.3 \text{ fb}^{-1}$ from the dijet signal region $115 < M_{jj} < 175 \text{ GeV}$ [2]. Left: Expected backgrounds and data; right: background subtracted data.

of this section. We will show that the threshold form of the ΔR and $\Delta\chi$ distributions provide direct measures of the velocity of the dijet system in the subprocess center-of-mass frame that are independent of measuring p/E and, thus, are independent checks on the two-resonance topology of the dijet's production mechanism.⁴ One might think that the corresponding $\Delta R_{\ell\ell}$ and $\Delta\chi_{\ell\ell}$ distributions from $Z \rightarrow \ell^+\ell^-$ would be similarly valuable. Unfortunately, because the dileptons come from real Z 's and our cuts make the background Z 's like the signal ones, $\Delta R_{\ell\ell}$ and $\Delta\chi_{\ell\ell}$ are indistinguishable from their backgrounds.

For our analysis, we assume the jets from π_T decay are massless. We have examined the effect of including jet masses and found them to be unimportant. We will remark briefly on them at the end of this section. We first consider the dominant ρ_T contribution to $W/Z\pi_T$ production, commenting on the a_T contribution also at the end.

Define the angles θ , θ^* and ϕ^* as follows: Choose the z -axis as the direction of the event's boost; this is usually the direction of the incoming quark in the subprocess c.m. frame. In the ρ_T rest frame, θ is the polar angle of the π_T velocity \mathbf{v} , the angle it makes with the z -axis. Define the xz -plane as the one containing the unit vectors \hat{z} and \hat{v} , so that $\hat{v} = \hat{x} \sin \theta + \hat{z} \cos \theta$, and $\hat{y} = \hat{z} \times \hat{x}$. Define a starred coordinate system *in the π_T rest frame* by making a rotation by angle θ about the y -axis of the ρ_T frame. This rotation takes \hat{z} into $\hat{z}^* = \hat{v}$ and \hat{x} into $\hat{x}^* = \hat{x} \cos \theta - \hat{z} \sin \theta$. In this frame, let \hat{p}_1^* be the unit vector in the

⁴Recall that $\Delta\chi$ is defined in the ρ_T rest frame, while ΔR is defined in the lab frame. If one wishes to remove the effect of $p_T(\rho_T)$ on ΔR , it should be defined in the ρ_T frame.

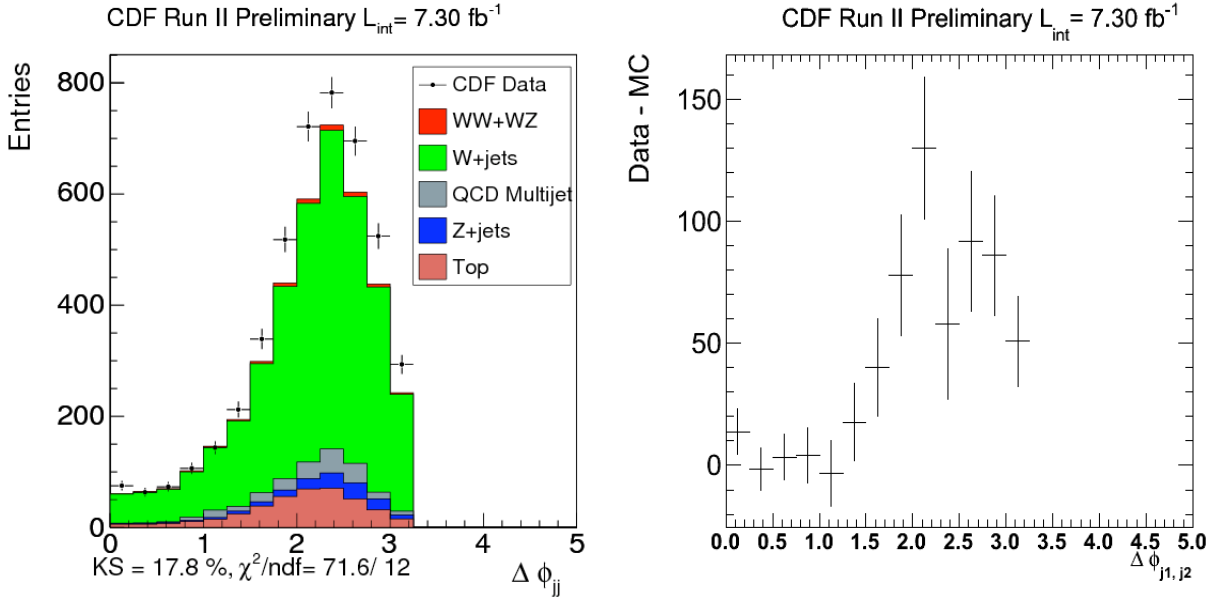


Figure 3: CDF $\Delta\phi$ distributions for $\int \mathcal{L} dt = 7.3 \text{ fb}^{-1}$ from the dijet signal region $115 < M_{jj} < 175 \text{ GeV}$ [2]. Left: Expected backgrounds and data; right: background subtracted data.

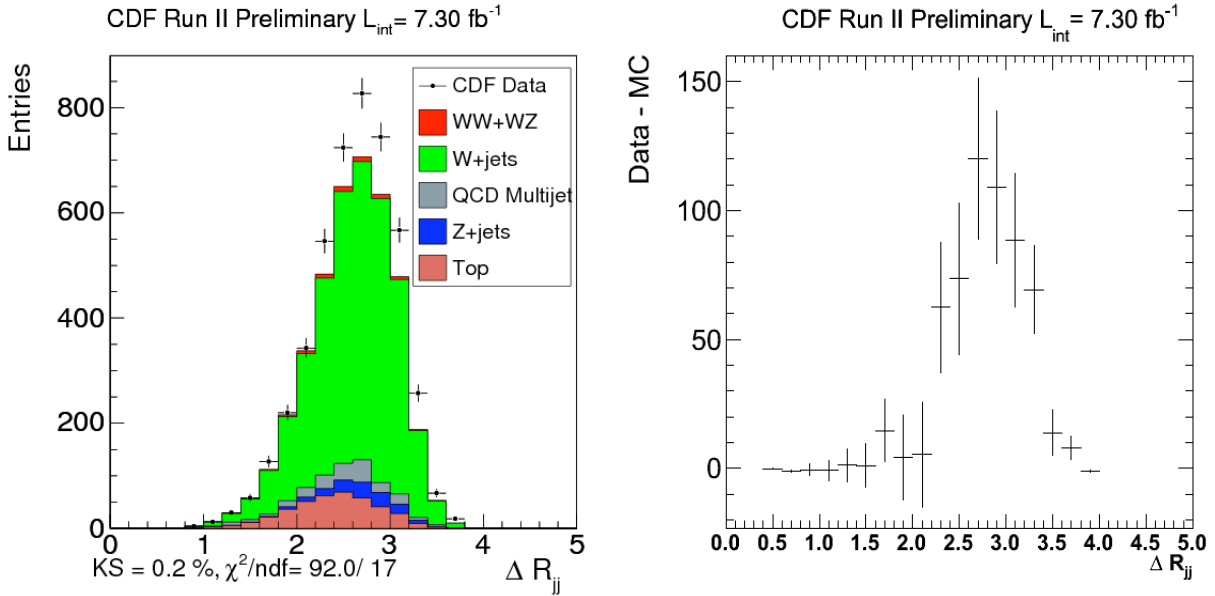


Figure 4: CDF ΔR distributions for $\int \mathcal{L} dt = 7.3 \text{ fb}^{-1}$ from the dijet signal region $115 < M_{jj} < 175 \text{ GeV}$ [2]. Left: Expected backgrounds and data; right: background subtracted data.

direction of the jet (parton) making the smaller angle with the direction of $\hat{\mathbf{v}}$. This angle is θ^* ; the azimuthal angle of $\mathbf{p}_1^* = -\mathbf{p}_2^*$ is ϕ^* :

$$\cos \theta = \hat{\mathbf{z}} \cdot \hat{\mathbf{v}}, \quad \cos \theta^* = \hat{\mathbf{p}}_1^* \cdot \hat{\mathbf{v}}, \quad \tan \phi^* = p_{1y}^*/p_{1x}^*. \quad (1)$$

Note that, since $\pi_T \rightarrow \bar{q}q$ is isotropic in its rest frame, the distribution $d\sigma(\bar{q}q \rightarrow \rho_T \rightarrow Wjj)/d(\cos \theta^*) = \sigma/2$, where σ is the total subprocess cross section.

It is easier to consider the $d\sigma/d(\Delta\chi)$ distribution first. For massless jets,

$$1 - \cos(\Delta\chi) = \frac{2(1 - v^2)}{1 - v^2 \cos^2 \theta^*}. \quad (2)$$

The minimum value of $\Delta\chi$ occurs when $\theta^* = \pi/2$ (i.e., $\mathbf{v} \perp \mathbf{p}_1^*$), and so

$$\pi \geq \Delta\chi \geq (\Delta\chi)_{\min} = 2 \cos^{-1}(v). \quad (3)$$

From Eq. (2), it is easy to see that

$$\frac{d\sigma}{d(\Delta\chi)} = \frac{(1 - v^2) \sigma}{4v \sin^2(\Delta\chi/2) \sqrt{\cos^2((\Delta\chi)_{\min}/2) - \cos^2((\Delta\chi)/2)}}, \quad (4)$$

i.e., the $\Delta\chi$ distribution has an inverse-square-root singularity at $\Delta\chi = (\Delta\chi)_{\min} = 2 \cos^{-1}(v) = 2.23$ for our input masses, and falls sharply above there. This is illustrated in Fig. 5 where we plot this distribution for the primary partons and for the reconstructed jets. The low-side tail for the jets is an artifact of their reconstruction.

To understand this singularity better, it follows from Eq. (2) that $\Delta\chi$ may be expanded about $\cos \theta^* = 0$ as

$$\Delta\chi = (\Delta\chi)_{\min} + \frac{a}{2} \cos^2 \theta^* + \dots, \quad (5)$$

where a is a positive v -dependent coefficient. Then, near $\cos \theta^* = 0$, i.e., the $\Delta\chi$ threshold,

$$\frac{d\sigma}{d(\Delta\chi)} = \frac{\sigma}{2} \frac{d(\cos \theta^*)}{d(\Delta\chi)} \propto \frac{1}{\sqrt{\Delta\chi - (\Delta\chi)_{\min}}}. \quad (6)$$

It is the simple one-variable Taylor expansion of $\Delta\chi$ in Eq. (5) that has caused this singularity.

The discussion of $d\sigma/d(\Delta R)$ for the LSTC signal shares some features with $d\sigma/d(\Delta\chi)$, though it is qualitatively different. The ΔR distribution also vanishes below a threshold, $(\Delta R)_{\min}$, which is equal to $(\Delta\chi)_{\min} = 2 \cos^{-1}(v)$. This remarkable feature, derived in the appendix, can be understood simply as a consequence of the fact that the minimum of ΔR occurs when *both* jet rapidities vanish. In that case, $\Delta R = \Delta\phi = \Delta\chi$.

At threshold, however, the ΔR distribution is $\propto \sqrt{\Delta R - (\Delta\chi)_{\min}}$, not the inverse square root. As illustrated in Fig. 5, it rises sharply from threshold into a broad feature before decreasing. The measure of the π_T velocity v is given by the onset of the rise, not its peak. This is the behavior seen in the CDF data in Fig. 4, where the rise starts very near

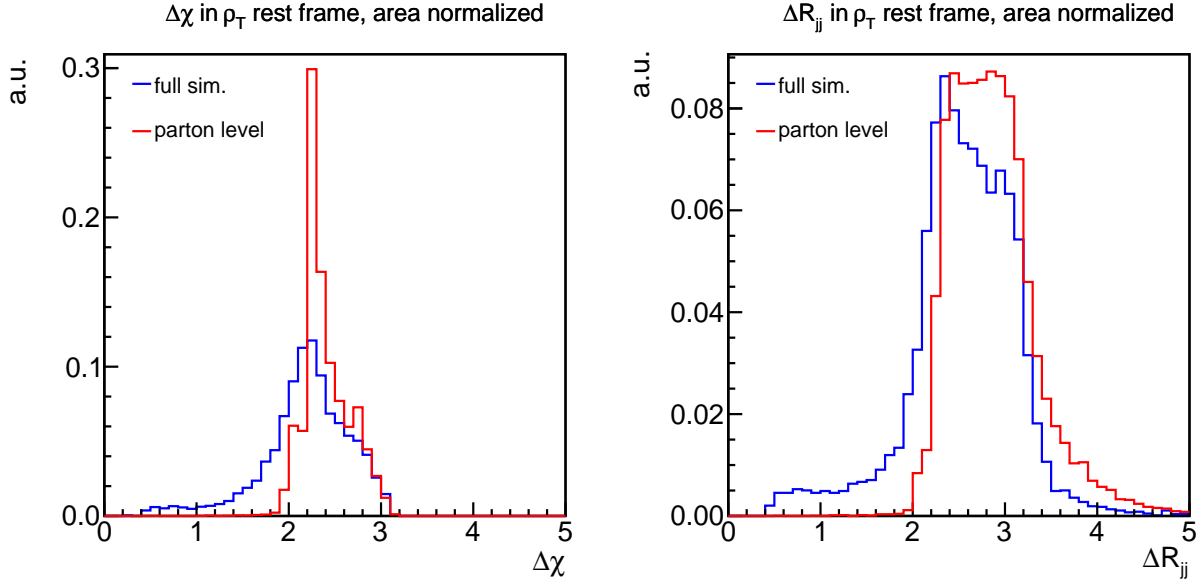


Figure 5: The area-normalized $\Delta\chi$ and ΔR distributions for the primary parton/jet in $\rho_T \rightarrow W\pi_T$ production followed by $\pi_T \rightarrow \bar{q}q$ decay, constructed as described in the text. Red: pure distribution of primary parton before any radiation; blue: the distribution for the jets reconstructed as described in Sec. 3.

$2 \cos^{-1}(v) = 2.23$ for our input masses. Both the $\Delta\chi$ and ΔR distributions measure the π_T velocity v and, therefore, provide confirmations of the $\rho_T \rightarrow W\pi_T$ hypothesis which are *independent* of the background under the M_{Wjj} resonant peak and of uncertainty in the \cancel{E}_T resolution as well.

The reason for this qualitative difference between the two distributions is that $d\sigma/\Delta\chi$ involves a one-dimensional trade of $\cos\theta^*$ for $\Delta\chi$, whereas ΔR is parametrized in terms of the three angles θ, θ^*, ϕ^* in an intricate way, with all three being integrated over to account for the constraint defining ΔR . In contrast to what happens in the $\Delta\chi$ case, the Jacobian singularity at the threshold is “antidifferentiated” twice, hence its comparatively lower strength. Using a Fadeev-Popov-like trick, the ΔR distribution can be written

$$\frac{d\sigma}{d(\Delta R)} = \int d(\cos\theta) d(\cos\theta^*) d(\cos\phi^*) \frac{d\sigma}{d(\cos\theta^*)} \delta(\Delta R - f(\cos\theta, \cos\theta^*, \cos\phi^*)) . \quad (7)$$

The function $f(\cos\theta, \cos\theta^*, \cos\phi^*)$ is shown in the appendix to have its absolute minimum at $\cos\theta = \cos\theta^* = \cos\phi^* = 0$, for which its value is equal to $(\Delta\chi)_{\min}$. Near its minimum it is locally parabolic and its Taylor expansion is

$$f(\cos\theta, \cos\theta^*, \cos\phi^*) = (\Delta\chi)_{\min} + \frac{1}{2} (b_\theta \cos^2\theta + b_{\theta^*} \cos^2\theta^* + b_{\phi^*} \cos^2\phi^*) + \dots \quad (8)$$

The positive v -dependent coefficients b_θ, b_{θ^*} and b_{ϕ^*} are also given in the appendix, Eq. (27). For ΔR close to $(\Delta\chi)_{\min}$, this expansion can be used to approximate Eq. (7). In a similar way

as for the $\Delta\chi$ distribution, integrating first over $\cos\theta^*$ generates the appearance of a Jacobian inverse square root singularity $\propto [2(\Delta R - (\Delta\chi)_{\min}) - (b_\theta \cos^2\theta + b_{\phi^*} \cos^2\phi^*)]^{-1/2}$. The two remaining integrations over $\cos\theta$ and $\cos\phi^*$ were trivial in the $\Delta\chi$ case as the integrand did not depend on them, but this is not so for ΔR which involves a double integration over a restricted angular phase space defined by

$$0 \leq b_\theta \cos^2\theta + b_{\phi^*} \cos^2\phi^* \leq 2(\Delta R - (\Delta\chi)_{\min}). \quad (9)$$

Performing the integral in Eq. (7) near $(\Delta R)_{\min} = (\Delta\chi)_{\min}$ yields a result $\propto \sqrt{\Delta R - (\Delta\chi)_{\min}}$.

We have examined the effect of finite jet masses (as opposed to jet reconstruction and energy resolution) on the threshold values of the ΔR and $\Delta\chi$ distributions and the extraction of the π_T velocity v from them. Our jets (which include b -jets) have masses $\lesssim 10$ GeV. Assuming, for simplicity, equal jet masses and denoting by $u = \sqrt{1 - 4M_{\text{jet}}^2/M_{\pi_T}^2}$ the jet velocity in the π_T rest frame, the corrected $(\Delta\chi)_{\min}(u)$ is

$$(\Delta\chi)_{\min}(u) = \cos^{-1} \frac{v^2 - u^2(1 - v^2)}{v^2 + u^2(1 - v^2)} \simeq \cos^{-1}(2v^2 - 1) - v(1 - v^2)^{1/2}(1 - u^2). \quad (10)$$

This is less than the massless $(\Delta\chi)_{\min}$ by half a percent for $M_{\text{jet}} = 15$ GeV.

Finally, as noted, the a_T accounts for about 25–30% of $W\pi_T$ production. This decay gives a π_T velocity of 2.00 in the a_T rest frame and $(\Delta\chi)_{\min} = 2.00$. The effect is clearly visible in the $\Delta\chi$ and ΔR distributions for the primary parton in Fig. 5, but is washed out by the low-end tails for the reconstructed jets. We believe that the low and high-end tails are due to the two π_T jets fragmenting to three jets and the two leading jets being closer or farther apart than the original pair.

3. The $\rho_T, a_T \rightarrow W\pi_T$ mode at the LHC

As a reminder, we assumed $M_{\rho_T} = 290$ GeV, $M_{a_T} = 1.1M_{\rho_T} = 320$ GeV, $M_{\pi_T} = 160$ GeV and $\sin\chi = 1/3$ to describe the CDF dijet excess. The Tevatron cross section is 2.2 pb. At the LHC, these parameters give $\sigma(W\pi_T) = 7.9$ pb (1.7 pb for $W \rightarrow e\nu, \mu\nu$). About 70% of the LHC rate is due to the ρ_T ; the ρ_T and a_T interference is very small. For such close masses, it is not possible to resolve the two resonances in the M_{Wjj} spectrum.

This past summer, the ATLAS Collaboration published dijet spectra for 1.02 fb^{-1} of Wjj data with exactly two jets and with two or more jets passing selection criteria [35]. The ATLAS cuts, designed to be as close to CDF's as possible, were: one isolated electron with $E_T > 25$ GeV or muon with $p_T > 20$ GeV and rapidity $|\eta_\ell| < 2.5$; $\cancel{E}_T > 25$ GeV and $M_T(W) > 40$ GeV; two (or more) jets with $p_T > 30$ GeV and $|\eta_j| < 2.8$; and $p_T(jj) > 40$ GeV and $\Delta\eta < 2.5$ for the two leading jets. The M_{jj} distribution for the two-jet data is shown in Fig. 6. There is no evidence of CDF's dijet excess near 150 GeV nor even of the standard model WW/WZ signal near 80 GeV. This is what we anticipated in Ref. [6] because of the great increase in Wjj backgrounds at the LHC relative to the Tevatron. On the other

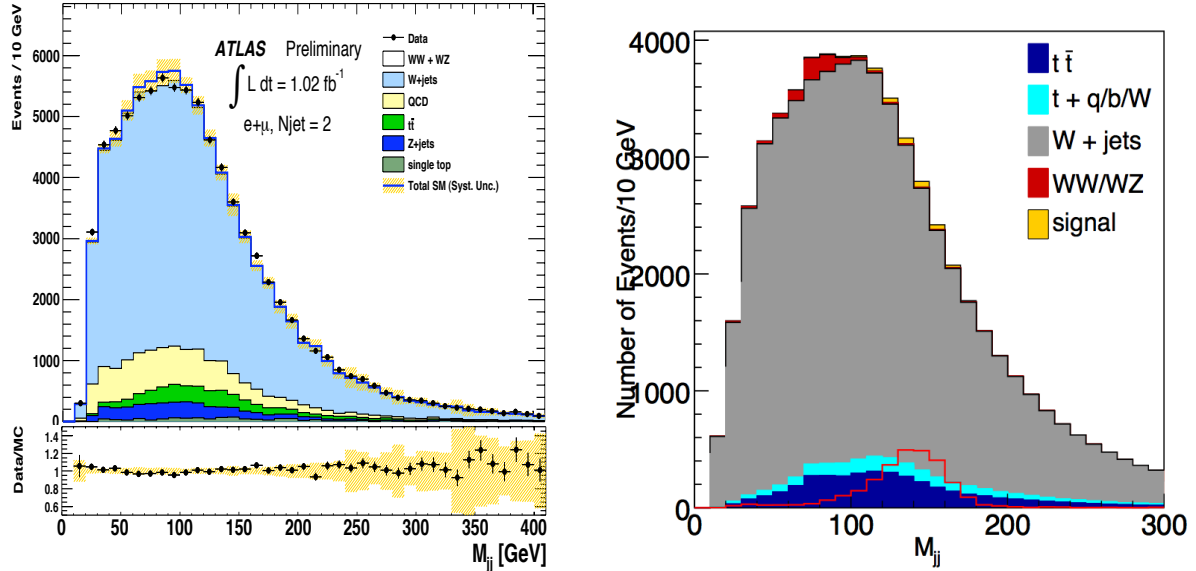


Figure 6: Left: The ATLAS M_{jj} distribution for exactly two jets and $\int \mathcal{L} dt = 1.02 \text{ fb}^{-1}$; from Ref. [35] Right: Simulation of Wjj production at the LHC with ATLAS cuts (except that $p_T(\ell) > 30 \text{ GeV}$) for 1.0 fb^{-1} . The open red histogram is the $\pi_T \rightarrow jj$ signal times 10.

hand, it is noteworthy and encouraging for future prospects that the ATLAS background simulation appears to fit the data well.

In Fig. 6 we also show an updated version of our simulation of the LSTC M_{jj} signal and backgrounds at the LHC for $\int \mathcal{L} dt = 1.0 \text{ fb}^{-1}$. ATLAS's cuts were used except that we required $p_T(\ell) > 30 \text{ GeV}$.⁵ This tighter cut and our inability to include the data-driven QCD background account for our lower event rate compared to ATLAS. Despite this, the agreement between the two is quite good. In particular, our simulation shows that the CDF/ATLAS cuts cannot reveal the LSTC interpretation of the CDF signal at the LHC for any reasonable luminosity.⁶

⁵Backgrounds were generated at matrix-element level using ALPGENv213 [36], then passed to PYTHIAv6.4 for showering and hadronization. We use CTEQ6L1 parton distribution functions and a factorization/renormalization scale of $\mu = 2M_W$ throughout. For the dominant W +jets background we generate $W + 2j$ (excl.) plus $W + 3j$ (inc.) samples, matched using the MLM procedure [37] (parton level cuts are imposed to ensure that $W + 0, 1$ jet events cannot contribute). After matching, the overall normalization is scaled to the NLO $W + jj$ value, calculated with MCFMv6 [38]. After passing through PYTHIA, final state particles are combined into (η, ϕ) cells of size 0.1×0.1 , and the energy in each cell smeared with $\Delta E/E = 1.0/\sqrt{E/\text{GeV}}$. The energy of each cell rescaled to make it massless. Isolated photons and leptons (e, μ) are removed, and all remaining cells with energy greater than 1 GeV are clustered into jets using FastJet (anti-kT algorithm, $R = 0.4$) [39]. Finally, the quadratic ambiguity in the W reconstruction was resolved by choosing the solution with the smaller $p_z(\nu)$.

⁶Models of the CDF signal that are gg -initiated or involve large coupling to heavier quarks, e.g., Ref. [26, 31], are likely excluded by the ATLAS data.

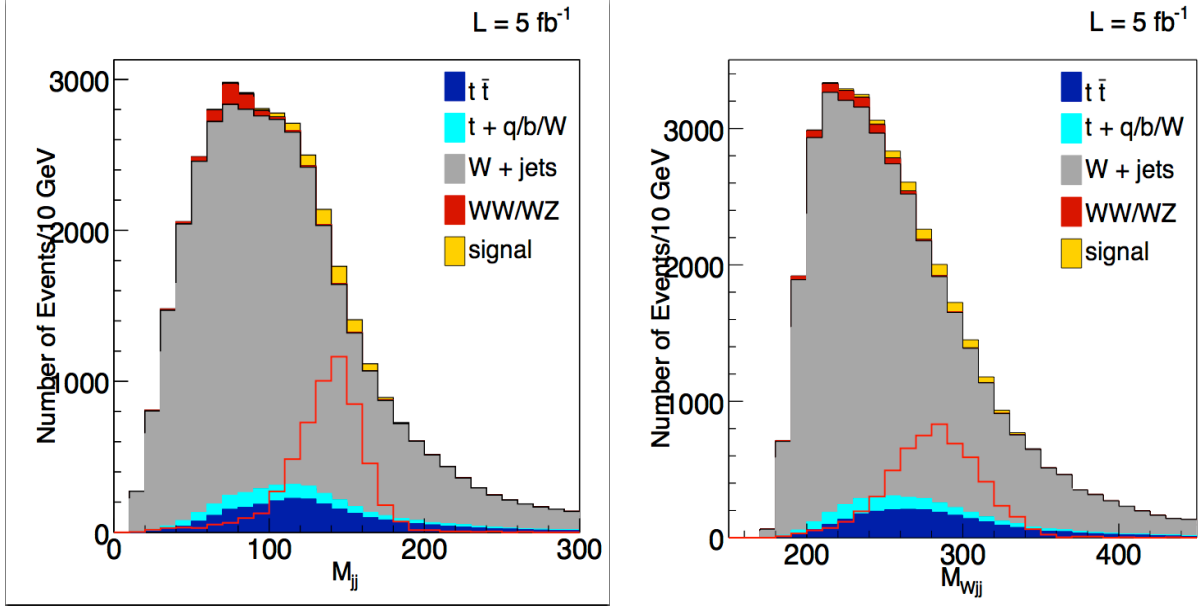


Figure 7: The M_{jj} and M_{Wjj} distributions of $\rho_T, a_T \rightarrow W\pi_T \rightarrow \ell\nu_\ell jj$ and backgrounds at the LHC for $\int \mathcal{L} dt = 5 \text{ fb}^{-1}$. Augmented ATLAS-like cuts as described in the text are employed. The open red histograms are the π_T and ρ_T signals times 10.

To improve the signal-to-background, we examined a variety of cuts motivated by $\rho_T \rightarrow W\pi_T$ kinematics. Cuts quite similar to those we proposed in Ref. [5] typically cause the background to peak very near the dijet resonance. To get the signal off the peak (and more like the original CDF M_{jj} excess [1]), we used the following cuts: lepton $p_T > 30 \text{ GeV}$ and rapidity $|\eta_\ell| < 2.5$, $\cancel{E}_T > 25 \text{ GeV}$, $M_T(W) > 40 \text{ GeV}$ and $p_T(W) > 60 \text{ GeV}$; exactly two jets with $p_{T1} > 40 \text{ GeV}$, $p_{T2} > 30 \text{ GeV}$, and $|\eta_j| < 2.8$; and $p_T(jj) > 45 \text{ GeV}$, $\Delta\eta < 1.2$; and $Q = M_{Wjj} - M_{jj} - M_W < 100 \text{ GeV}$. The M_{jj} and M_{Wjj} distributions are shown in Fig. 7 for $\int \mathcal{L} dt = 5 \text{ fb}^{-1}$. Counting events in the range $120 < M_{jj} < 170 \text{ GeV}$ gives $S/\sqrt{B} = 6.5$ but only $S/B = 0.050$ for this luminosity. Likewise, the ΔR and $\Delta\chi$ signals are very small and not useful. This is not promising. Perhaps with $20\text{--}30 \text{ fb}^{-1}$ a convincing signal could be seen in the Wjj data, but it would require a very good understanding of the backgrounds.

4. The $\rho_T^\pm, a_T^\pm \rightarrow Z\pi_T^\pm$ mode

Observation of $\rho_T^\pm, a_T^\pm \rightarrow Z\pi_T^\pm$, the isospin partner of the $W\pi_T^0$ decay mode, will be an important confirmation of CDF's Wjj signal. At the LHC, we predict $\sigma(\rho_T^\pm, a_T^\pm \rightarrow Z\pi_T^\pm) = 2.5 \text{ pb}$, lower than $\sigma(\rho_T^\pm, a_T^\pm \rightarrow W\pi_T^0) = 3.4 \text{ pb}$ because of the reduced phase space, $\propto p^3$. Then, $\sigma(\rho_T^\pm, a_T^\pm \rightarrow Z\pi_T \rightarrow \ell^+\ell^- jj) = 155 \text{ fb}$ for $\ell = e$ and μ . This is about 10% of the total $W\pi_T \rightarrow \ell\nu_\ell jj$ signal. We might, therefore, expect that ~ 10 times the luminosity needed for the $W\pi_T$ signal would be required for the same sensitivity to $Z\pi_T$. Actually, because there

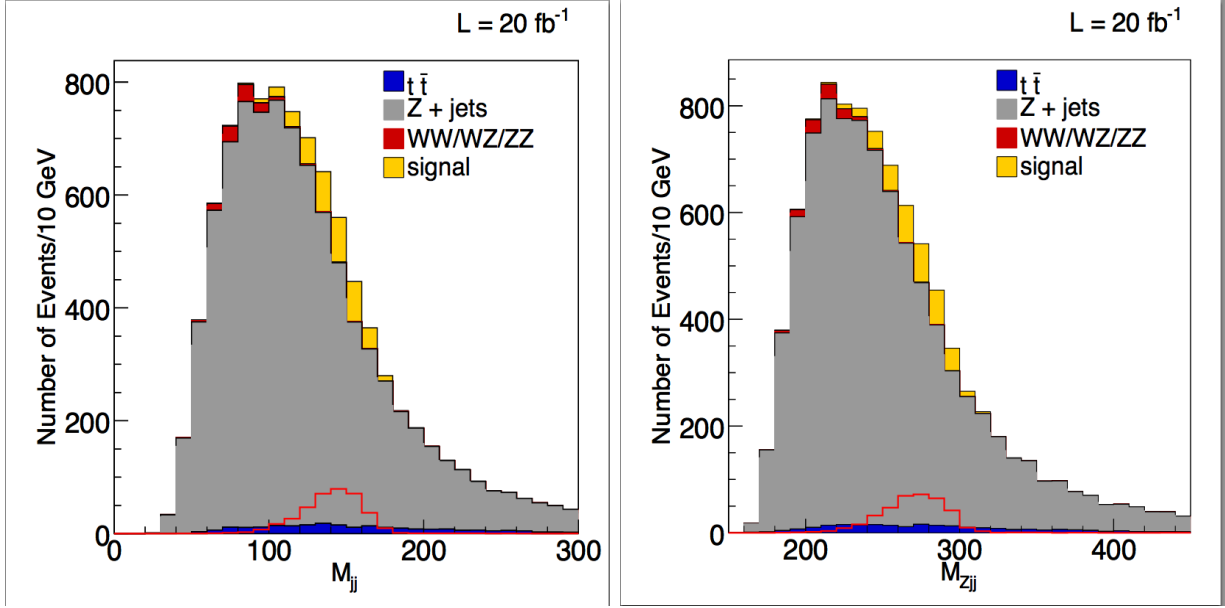


Figure 8: The M_{jj} and M_{Zjj} distributions of $\rho_T^\pm, a_T^\pm \rightarrow Z\pi_T^\pm \rightarrow \ell^+\ell^-jj$ and backgrounds at the LHC for $\int \mathcal{L}dt = 20 \text{ fb}^{-1}$. The cuts used are described in the text. The open red histograms are the unscaled π_T and ρ_T signals.

is no QCD multijet background nor \cancel{E}_T resolution to pollute the Zjj data, the situation is better than this.

Figure 8 shows the $Z\pi_T$ signal and its background, almost entirely from $Z + \text{jets}$, for $\int \mathcal{L}dt = 20 \text{ fb}^{-1}$. The cuts used here are: two electrons or muons of opposite charge with $p_T > 30 \text{ GeV}$, $|\eta_\ell| < 2.5$, $60 < M_{\ell^+\ell^-} < 100 \text{ GeV}$ and $p_T(Z) > 50 \text{ GeV}$; exactly two jets with $p_T > 30 \text{ GeV}$ and $|\eta_j| < 2.8$; $p_T(jj) > 40 \text{ GeV}$, $\Delta\eta < 1.75$ and $Q = M_{Zjj} - M_{jj} - M_Z < 60 \text{ GeV}$. This Q -cut is very important in reducing the background.⁷ These give $S/\sqrt{B} = 6.0$ and $S/B = 0.13$ for the dijet signal in $120 < M_{jj} < 170 \text{ GeV}$. The figure also shows the M_{Zjj} distribution; it has $S/\sqrt{B} = 5.8$ and $S/B = 0.11$ for $250 < M_{Zjj} < 320 \text{ GeV}$. These signal-to-background rates and the position of the dijet signal on the falling backgrounds are similar to those in Ref. [2]. Therefore, if our interpretation of the CDF dijet excess is correct, both $\pi_T \rightarrow jj$ and $\rho_T \rightarrow \ell^+\ell^-jj$ should be observable in the data to be collected at the LHC in 2012.

Figure 9 shows the ΔR and $\Delta\chi$ distributions for $\rho_T, a_T \rightarrow Z\pi_T \rightarrow \ell^+\ell^-jj$. The skyscraper-shaped $\Delta\chi$ distribution is interesting. The background peaks at $\Delta\chi \simeq 2.3$, and appears rather symmetrical about this point except that its high side falls more rapidly above 2.7 because $(\Delta\chi)_{\text{max}} = \pi$. The signal's $\Delta\chi$ distribution sits atop the skyscraper, concentrated in about 175 events in a Chrysler Building-like spire⁸ at $\Delta\chi = 2.2\text{--}2.3$, whereas

⁷ $\rho_T, a_T \rightarrow WZ \rightarrow \ell^+\ell^-jj$ is included in this simulation, but it is removed by the Q -cut.

⁸http://en.wikipedia.org/wiki/Chrysler_Building

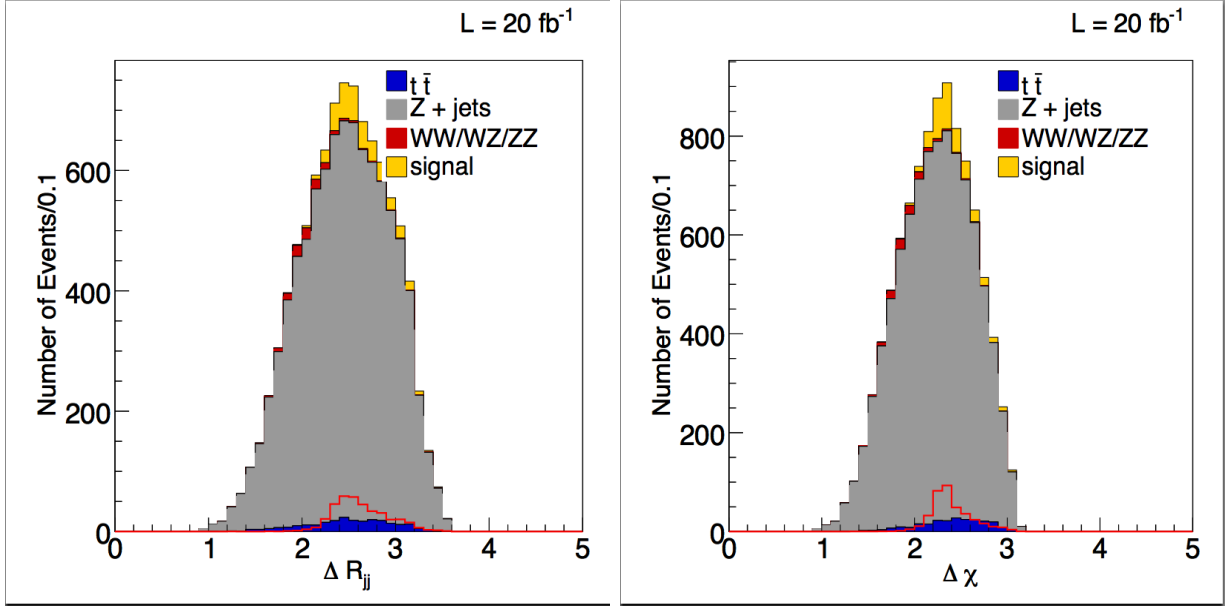


Figure 9: The ΔR and $\Delta\chi$ distributions for $\rho_T^\pm, a_T^\pm \rightarrow Z\pi_T^\pm \rightarrow \ell^+\ell^-jj$ and backgrounds at the LHC for $\int \mathcal{L} dt = 20 \text{ fb}^{-1}$. The cuts used are described in the text. The open red histograms are the unscaled signals.

the theoretical $(\Delta\chi)_{\min} = 2 \cos^{-1}(v) = 2.31$ for $\rho_T \rightarrow Z\pi_T$. This is just as expected when the effects of jet reconstruction and $a_T \rightarrow Z\pi_T$ are taken into account; see Fig. 5. If the actual $\Delta\chi$ data, with our cuts, has the shape of our simulation, we believe the signal spire excess can be observed. Similar remarks apply to the shape and observability of the slightly broader ΔR distribution in Fig. 9.

5. The $\rho_T^\pm, a_T^\pm \rightarrow WZ$ mode

Finally, the decay channel $\rho_T^\pm, a_T^\pm \rightarrow W^\pm Z$ furnishes another important check on the LSTC hypothesis provided that $\sin\chi \gtrsim 1/4$. The dominant contribution, $\rho_T \rightarrow W_L Z_L$, has an angular distribution $\propto \sin^2\theta$ so that the production is fairly central. We expect $\sigma(\rho_T, a_T \rightarrow WZ)/\sigma(\rho_T, a_T \rightarrow W\pi_T^0) \simeq (p(Z)/p(\pi_T))^3 \tan^2\chi$. The PYTHIA rates are roughly consistent with this. For our input masses and $\sin\chi = (\frac{1}{4}, \frac{1}{3}, \frac{1}{2})$, we obtain

$$\sigma(\rho_T, a_T \rightarrow WZ \rightarrow \ell^+\ell^-\ell^\pm\nu_\ell) = (13, 21, 44) \text{ fb}, \quad (11)$$

$$\sigma(\rho_T, a_T \rightarrow WZ \rightarrow \ell^+\ell^-jj) = (42, 67, 140) \text{ fb}, \quad (12)$$

$$\sigma(\rho_T, a_T \rightarrow Z\pi_T \rightarrow \ell^+\ell^-jj) = (165, 155, 120) \text{ fb}, \quad (13)$$

for $\ell = e, \mu$.

The $\rho_T, a_T \rightarrow \ell^+\ell^-\ell^\pm\nu_\ell$ mode has been discussed in Refs. [18, 19]. It has the advantages of cleanliness and freedom from jet uncertainties (except \cancel{E}_T resolution). Standard-model

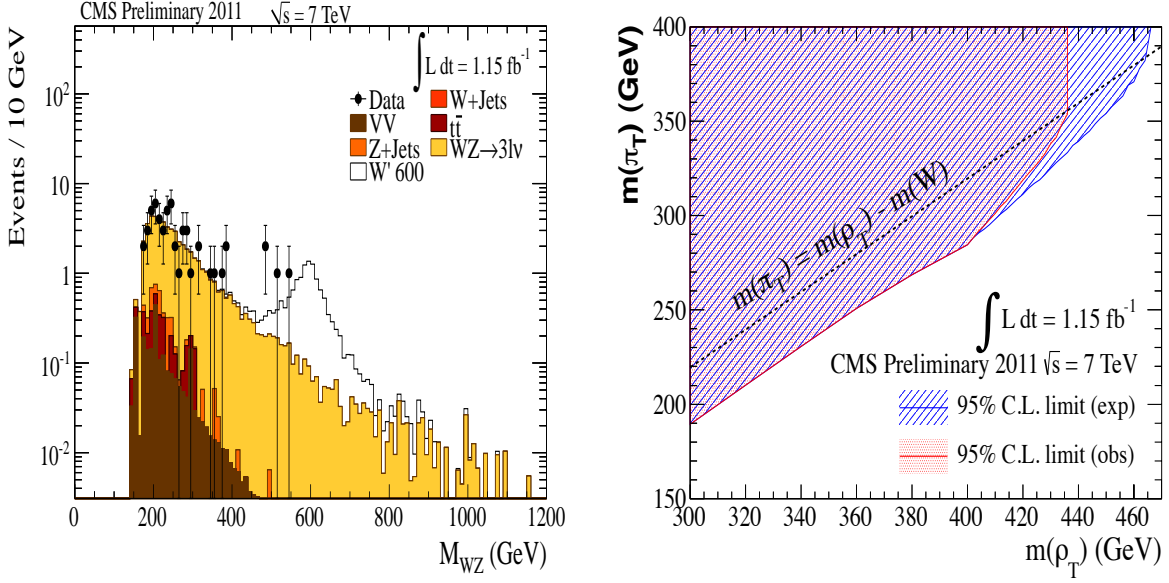


Figure 10: Left: WZ invariant mass distribution after the WZ candidate selection has been optimized for the search for a W' with mass of 600 GeV. Right: Exclusion plot for LSTC as described in the text. From the CMS Collaboration, Ref. [41]

WZ production at the LHC peaks at $M_{WZ} = 300 \text{ GeV} \simeq M_{\rho_T}$ and this is the dominant background to the $3\ell\nu$ signal. The DØ collaboration searched for this channel for the standard LSTC parameters including $\sin \chi = 1/3$, and excluded it at 95% C.L. up to $M_{\rho_T} \simeq 400 \text{ GeV}$ so long as the $\rho_T \rightarrow W\pi_T$ channel is closed [40]. The CMS Collaboration recently reported a search for a sequential standard model W' and for $\rho_T, a_T \rightarrow WZ \rightarrow 3\ell\nu$ using 1.15 fb^{-1} of 7 TeV data [41]. The M_{WZ} spectrum and M_{ρ_T} vs. M_{π_T} exclusion plot are shown in Fig. 10. Standard LSTC parameters, including $\sin \chi = 1/3$ were used for this plot. Extrapolating it rules out $(M_{\rho_T} = 290 \text{ GeV}, M_{\pi_T} = 180 \text{ GeV})$ at 95%. It appears that $5\text{--}10 \text{ fb}^{-1}$ will be sufficient to exclude our CDF/LSTC mass point of $(290, 160) \text{ GeV}$ for $\sin \chi \gtrsim 1/3$.

The dominant background to $\rho_T, a_T \rightarrow WZ \rightarrow \ell^+\ell^-jj$ is $Z + \text{jets}$. As can be inferred from Fig. 6 for Wjj production with ATLAS/CDF cuts, the signal will sit at the top of the M_{jj} spectrum. This is what makes the dijet signal in $WW/WZ \rightarrow \ell\nu jj$ so difficult to see. On the plus side, since the LSTC and standard model diboson processes have very similar production characteristics, the two signals can be seen with the same cuts and will coincide. We simulated this mode and found what may be a promising set of cuts to extract the $W \rightarrow jj$ signal. The basic cuts used for the Zjj signal in Sec. 4 were adopted except that we required $p_T(Z) > 100 \text{ GeV}$, $p_T(jj) > 70 \text{ GeV}$ and $110 < Q = M_{Zjj} - M_W - M_Z < 150 \text{ GeV}$. The mass distributions for $\sin \chi = 1/3$ are shown in Fig. 11 for $\int \mathcal{L} dt = 20 \text{ fb}^{-1}$. The LSTC signal more than doubles the number of standard model $W \rightarrow jj$ events in the M_{jj} distribution and it appears that the dijet signal should be observable with such a

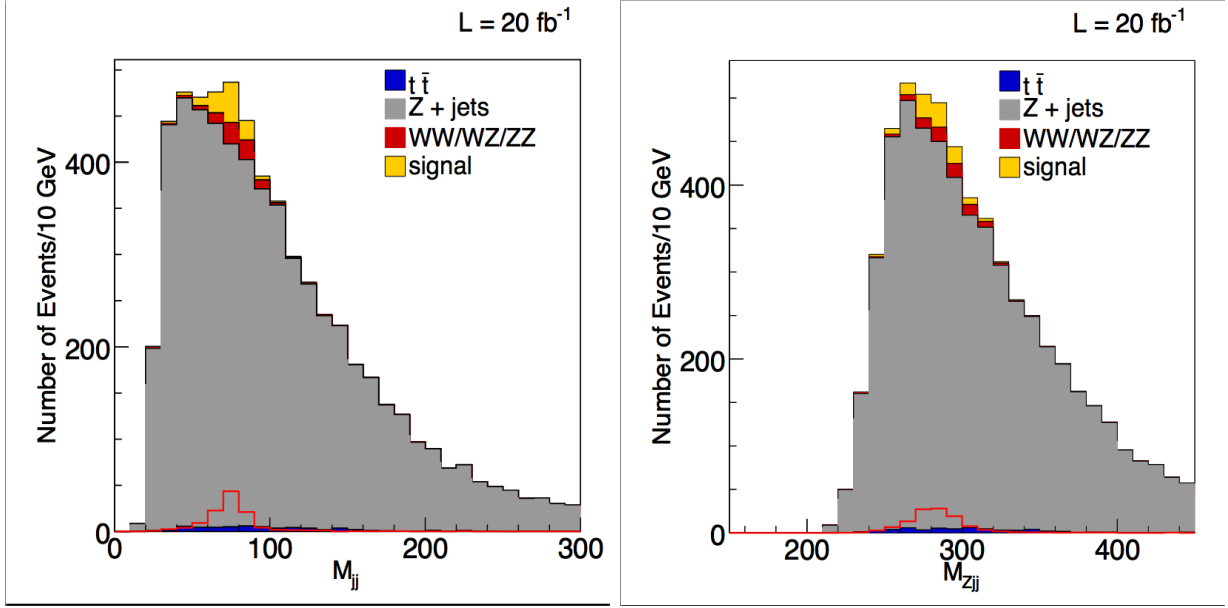


Figure 11: The M_{jj} and M_{Zjj} distributions of $\rho_T^\pm, a_T^\pm \rightarrow WZ \rightarrow \ell^+\ell^-jj$ and backgrounds at the LHC for $\int \mathcal{L} dt = 20 \text{ fb}^{-1}$. The cuts used are described in the text. The open red histograms are the unscaled π_T and ρ_T signals.

data set. Including the standard diboson events gives $S/\sqrt{B} = 4.1$ and $S/B = 0.10$ for $60 < M_{jj} < 100 \text{ GeV}$. The M_{Zjj} signal is problematic, but it may be possible to combine its significance with that for $\rho_T, a_T \rightarrow Z\pi_T \rightarrow \ell^+\ell^-jj$. The ΔR and $\Delta\chi$ distributions are in Fig. 12. The narrow LSTC signal and the diboson contribution both peak very near $(\Delta\chi)_{\min} = 2 \cos^{-1}(v_W) = 1.21$ and they should be observable as well.

Acknowledgments

We are grateful to K. Black, T. Bose, P. Catastini, V. Cavaliere, C. Fantasia and M. Mangano for valuable conversations and advice. This work was supported by Fermilab operated by Fermi Research Alliance, LLC, U.S. Department of Energy Contract DE-AC02-07CH11359 (EE and AM) and in part by the U.S. Department of Energy under Grant DE-FG02-91ER40676 (KL). KL's research was also supported in part by Laboratoire d'Annecy-le-Vieux de Physique Theorique (LAPTh) and the CERN Theory Group and he thanks LAPTh and CERN for their hospitality.

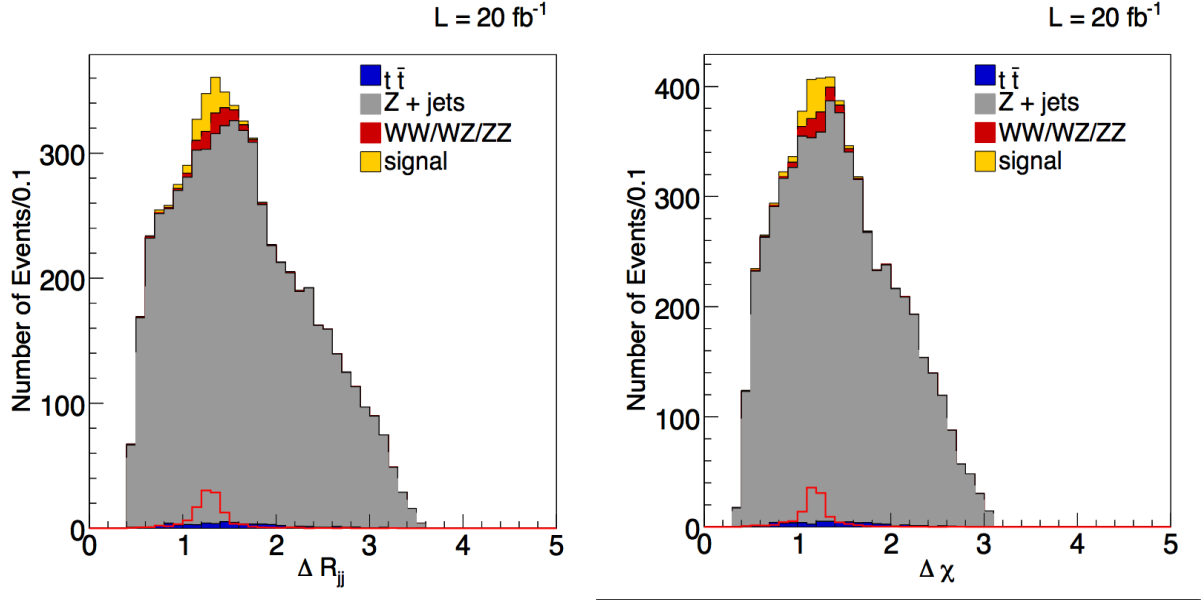


Figure 12: The ΔR and $\Delta\chi$ distributions of $\rho_T^\pm, a_T^\pm \rightarrow WZ \rightarrow \ell^+\ell^-jj$ and backgrounds at the LHC for $\int \mathcal{L} dt = 20 \text{ fb}^{-1}$. The cuts used are described in the text. The open red histograms are the unscaled signals.

Appendix: Nonanalytic Threshold Behavior of $d\sigma/d(\Delta R)$

1. Kinematics

We recall first the definition of the angles θ , θ^* , ϕ^* and the relevant coordinate systems. Choose the z -axis as the direction of the incoming quark in the subprocess c.m. frame (or the direction of the harder initial-state parton in the pp collision). In the ρ_T (or a_T) rest frame, θ is the polar angle of the π_T velocity \mathbf{v} , the angle it makes with the z -axis. Define the xz -plane as the one containing the unit vectors $\hat{\mathbf{z}}$ and $\hat{\mathbf{v}}$, so that $\hat{\mathbf{v}} = \hat{\mathbf{x}} \sin \theta + \hat{\mathbf{z}} \cos \theta$, and $\hat{\mathbf{y}} = \hat{\mathbf{z}} \times \hat{\mathbf{x}}$. Define a starred coordinate system *in the π_T rest frame* by making a rotation by angle θ about the y -axis of the ρ_T frame. This rotation takes $\hat{\mathbf{z}}$ into $\hat{\mathbf{z}}^* = \hat{\mathbf{v}}$ and $\hat{\mathbf{x}}$ into $\hat{\mathbf{x}}^* = \hat{\mathbf{x}} \cos \theta - \hat{\mathbf{z}} \sin \theta$. In this frame, let $\hat{\mathbf{p}}_1^*$ be the unit vector in the direction of the jet (parton) making the smaller angle with the direction of $\hat{\mathbf{v}}$. This angle is θ^* ; the azimuthal angle of $\mathbf{p}_1^* = -\mathbf{p}_2^*$ is ϕ^* :

$$\cos \theta = \hat{\mathbf{z}} \cdot \hat{\mathbf{v}}, \quad \cos \theta^* = \hat{\mathbf{p}}_1^* \cdot \hat{\mathbf{v}}, \quad \tan \phi^* = p_{1y}^*/p_{1x}^*. \quad (14)$$

The jets from π_T decay are labeled $j = 1, 2$ and they are assumed massless. Let $\zeta_1 = +$ and $\zeta_2 = -$, and $c_\theta = \cos \theta$, $s_\theta = \sin \theta$, etc. The boosted jets in the lab frame are

$$\begin{aligned} p_j^0 &= \frac{1}{2} M_{\pi_T} \gamma (1 + \zeta_j v c_{\theta^*}), \\ \mathbf{p}_{j\parallel} &= \frac{1}{2} M_{\pi_T} \gamma (v + \zeta_j c_{\theta^*}) (\hat{\mathbf{x}} s_\theta + \hat{\mathbf{z}} c_\theta), \\ \mathbf{p}_{j\perp} &= \frac{1}{2} M_{\pi_T} \zeta_j ((\hat{\mathbf{x}} c_\theta - \hat{\mathbf{z}} s_\theta) s_{\theta^*} c_{\phi^*} + \hat{\mathbf{y}} s_{\theta^*} s_{\phi^*}), \end{aligned} \quad (15)$$

where $\gamma = (1 - v^2)^{-\frac{1}{2}}$.

We want to find the minimum of $\Delta R = \sqrt{(\Delta\eta)^2 + (\Delta\phi)^2}$ as a function of c_θ , c_{θ^*} and c_{ϕ^*} . From Eq. (15),

$$\Delta\eta = \frac{1}{2} \ln \left[\left(\frac{1 + vc_{\theta^*} + (v + c_{\theta^*})c_\theta - \gamma^{-1}s_{\theta^*}c_{\phi^*}s_\theta}{1 + vc_{\theta^*} - (v + c_{\theta^*})c_\theta + \gamma^{-1}s_{\theta^*}c_{\phi^*}s_\theta} \right) \times \left(\frac{1 - vc_{\theta^*} - (v - c_{\theta^*})c_\theta - \gamma^{-1}s_{\theta^*}c_{\phi^*}s_\theta}{1 - vc_{\theta^*} + (v - c_{\theta^*})c_\theta + \gamma^{-1}s_{\theta^*}c_{\phi^*}s_\theta} \right) \right], \quad (16)$$

and

$$\begin{aligned} \cos(\Delta\phi) &= \frac{\mathbf{p}_{T1} \cdot \mathbf{p}_{T2}}{p_{T1} p_{T2}} \\ &= \frac{v^2 s_\theta^2 - (c_{\theta^*}^2 s_\theta^2 + \gamma^{-2} s_{\theta^*}^2 (c_\theta^2 c_{\phi^*}^2 + s_{\phi^*}^2)) - 2\gamma^{-1} s_{\theta^*} c_{\theta^*} s_\theta c_\theta c_{\phi^*}}{\left\{ [v^2 s_\theta^2 + (c_{\theta^*} s_\theta + \gamma^{-1} s_{\theta^*} c_{\phi^*} c_\theta)^2 + (\gamma^{-1} s_{\theta^*} s_{\phi^*})^2]^2 - 4v^2 s_\theta^2 (c_{\theta^*} s_\theta + \gamma^{-1} s_{\theta^*} c_{\phi^*} c_\theta)^2 \right\}^{1/2}}. \end{aligned} \quad (17)$$

2. Minimum of ΔR

It clearly is hopeless to deal with the analytic expression of ΔR as a function of c_θ , c_{θ^*} , c_{ϕ^*} . However, there is a simple way to bypass it. The quantity

$$\Delta \equiv \frac{M_{\pi T}^2}{2p_{T1} p_{T2}} = \cosh(\Delta\eta) - \cos(\Delta\phi), \quad (18)$$

with $\Delta\eta \geq 0$ and $0 \leq \Delta\phi \leq \pi$, is a monotonically increasing function of ΔR . This is seen by parametrizing

$$\Delta\eta = \Delta R \cos \lambda, \quad \Delta\phi = \Delta R \sin \lambda \quad (19)$$

with $\lambda \geq 0$ and $\lambda \leq \pi/2$ if $\Delta R \leq \pi$ or $\lambda \leq \sin^{-1}(\pi/\Delta R)$ if $\Delta R > \pi$. Then

$$\frac{\partial \Delta}{\partial (\Delta R)} = \cos \lambda \sinh(\Delta\eta) + \sin \lambda \sin(\Delta\phi). \quad (20)$$

This is non-negative. It vanishes only for (1) $\Delta R = 0$, which means $\Delta = 0$, and this cannot happen by its definition, Eq. (18), and for (2) $\Delta\eta = 0$, $\Delta\phi = \pi$ meaning $\Delta R = \pi$; the latter is a saddle point. This is the ‘‘Col du Delta’’, but it is one-sided, as shown in Fig. 13.

Minimizing ΔR thus amounts to minimizing Δ , which in turn, amounts to maximizing $p_{T1} p_{T2}$. This is much simpler to examine than the original problem. We first maximize $p_{T1} p_{T2}$ at fixed c_{θ^*} , then maximize it with respect to c_{θ^*} . Since $p_{Tj} = \sqrt{p_{j0}^2 - p_{jz}^2}$ and p_{j0} depends only on c_{θ^*} , p_{T1} and p_{T2} are separately maximized at fixed c_{θ^*} when $p_{1z} = p_{2z} = 0$. This requires $c_\theta = s_\theta c_{\phi^*} = 0$. Then $p_{T1} p_{T2} = (\frac{1}{2}\gamma M_{\pi T})^2 (1 - v^2 \cos^2 \theta^*)$ is maximized at $c_{\theta^*} = 0$. In conclusion, ΔR is minimized if and only if

$$c_\theta = c_{\theta^*} = c_{\phi^*} = 0. \quad (21)$$

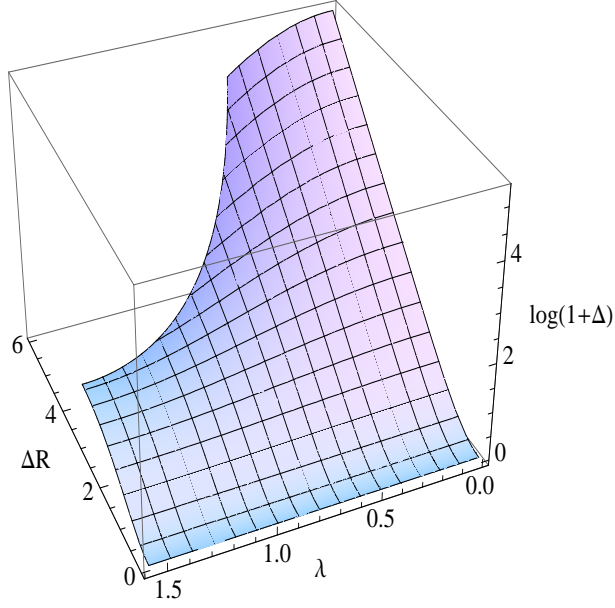


Figure 13: The function $\ln(1 + \Delta)$ defined in Eqs. (18,20). The Col du Delta at $\lambda = \pi/2$, $\Delta R = \pi$ is approached along the road $\lambda = \pi/2$. One cannot go over the pass and down the other side for the border is impassable. One must keep climbing along the ridge of increasing ΔR or return via the approach road.

This corresponds to two distinct, isolated points in the angular phase space ($\phi^* = \pi/2, 3\pi/2$). The degeneracy of the minimum is only discrete. At ΔR 's minimum, $\Delta\eta = 0$ and $\Delta\phi = \cos^{-1}(2v^2 - 1) = 2 \cos^{-1}(v) \equiv (\Delta\chi)_{\min}$, so that

$$(\Delta R)_{\min} = (\Delta\chi)_{\min} = 2 \cos^{-1}(v). \quad (22)$$

3. Local behavior around $\cos \theta = \cos \theta^* = \cos \phi^* = 0$

We now investigate the behavior of ΔR as a function of c_θ, c_{ϕ^*} and c_{θ^*} around its minimum at $c_\theta = c_{\theta^*} = c_{\phi^*} = 0$ by means of a Taylor expansion of at most second order in any of these variables. From, Eqs. (16,17), we obtain

$$\begin{aligned} (\Delta\eta)^2 &= 4\gamma^{-2}c_{\phi^*}^2 + \mathcal{O}(c^3), \\ \cos(\Delta\phi) &= \cos(\Delta\chi)_{\min} - (1 - \cos(\Delta\chi)_{\min})v^2(c_\theta^2 + c_{\theta^*}^2) + (1 + \cos(\Delta\chi)_{\min})\gamma^{-2}c_{\phi^*}^2 + \mathcal{O}(c^3). \end{aligned} \quad (23)$$

Interpreting the latter equation as:

$$\cos(\Delta\phi) = \cos(\Delta\chi)_{\min} - \sin(\Delta\chi)_{\min} (\Delta\phi - (\Delta\chi)_{\min}) + \mathcal{O}((\Delta\phi - (\Delta\chi)_{\min})^2) \quad (24)$$

we identify

$$\Delta\phi = (\Delta\chi)_{\min} + [v^2 \tan((\Delta\chi)_{\min}/2) (c_\theta^2 + c_{\theta^*}^2) - \gamma^{-2} \cot((\Delta\chi)_{\min}/2) c_{\phi^*}^2 + \mathcal{O}(c^3)]. \quad (25)$$

Then

$$\Delta R \equiv \sqrt{(\Delta\eta)^2 + (\Delta\phi)^2} = (\Delta\chi)_{\min} + \frac{1}{2} (b_\theta c_\theta^2 + b_{\theta^*} c_{\theta^*}^2 + b_{\phi^*} c_{\phi^*}^2) + \mathcal{O}(c^3), \quad (26)$$

where

$$\begin{aligned} b_\theta &= b_{\theta^*} = 2v^2 \tan((\Delta\chi)_{\min}/2) = 2v\gamma^{-1}, \\ b_{\phi^*} &= 2\gamma^{-2}(2/(\Delta\chi)_{\min} - v\gamma). \end{aligned} \quad (27)$$

The shape of the surface $\Delta R = f(c_\theta, c_{\theta^*}, c_{\phi^*})$ in the neighborhood of the minimum $\Delta R = \Delta\chi_{\min}$ is a convex paraboloid with ellipsoidal section whose eigen-directions are parallel to the axes of the coordinates c_θ , c_{θ^*} and c_{ϕ^*} . The curvature is > 0 along each of these axes for all $0 < v < 1$; i.e. there is no flat direction, as expected from the fact the minimum is at isolated point(s).

4. Calculation of the singular part of $d\sigma/d(\Delta R)$

The differential cross section for $\bar{q}q \rightarrow \rho_T, a_T \rightarrow W/Z\pi_T$, followed by $\pi_T \rightarrow \bar{q}q$ is ⁹

$$d\sigma = \left[\frac{d\sigma(\bar{q}q \rightarrow W/Z\pi_T)}{dc_\theta} \right] B(\pi_T \rightarrow \bar{q}q) \underbrace{\left[\frac{1}{\Gamma(\pi_T \rightarrow \bar{q}q)} \frac{d\Gamma(\pi_T \rightarrow \bar{q}q)}{dc_{\theta^*} dc_{\phi^*}} \right]}_{(2\pi\sqrt{1-c_{\phi^*}^2})^{-1}} dc_\theta dc_{\theta^*} dc_{\phi^*}. \quad (28)$$

To compute the distribution in a compound variable ζ , such as $\Delta\chi$ or ΔR , we use a Fadeev-Popov-like trick

$$1 = \int d\zeta \delta(\zeta - f(c_\theta, c_{\theta^*}, c_{\phi^*})). \quad (29)$$

where $f(c_\theta, c_{\theta^*}, c_{\phi^*})$ gives the expression of ζ in terms of the phase space variables. The ζ -distribution is then

$$\frac{d\sigma}{d\zeta} = \int d\sigma(\text{from Eq. (28)}) \delta(\zeta - f(c_\theta, c_{\theta^*}, c_{\phi^*})). \quad (30)$$

Let $\zeta = \Delta R$ be slightly above and close to $(\Delta\chi)_{\min}$, and define $\omega = \Delta R - (\Delta\chi)_{\min}$ to shorten expressions. Solving Eq. (26) with respect to c_{θ^*} gives

$$c_{\theta^*} = \pm \hat{c}_{\theta^*} = \pm \sqrt{\left(\frac{2}{b_{\theta^*}}\right) \left(\omega - \frac{1}{2}(b_\theta c_\theta^2 + b_{\phi^*} c_{\phi^*}^2) + \mathcal{O}(c^3)\right)}. \quad (31)$$

Notice that Eq. (31) has to be supplemented by the restriction

$$\omega - \frac{1}{2}(b_\theta c_\theta^2 + b_{\phi^*} c_{\phi^*}^2 + \mathcal{O}(c^3)) \geq 0. \quad (32)$$

⁹Since there are two points in the $(c_\theta, c_{\theta^*}, c_{\phi^*})$ phase space where ΔR has a minimum, $\theta = \theta^* = \pi/2$ and $\phi^* = \pi/2, 3\pi/2$, it is more convenient to use the variable c_{ϕ^*} instead of ϕ^* . This introduces (a) the Jacobian $(1 - c_{\phi^*}^2)^{-1/2}$ which is one at $c_{\phi^*} = 0$; and (b) a factor of two to account for the contributions of the two minima in the calculation of the normalization coefficient.

Substituting

$$\delta(\Delta R - f(c_\theta, c_{\theta^*}, c_{\phi^*})) = (b_{\theta^*} \hat{c}_{\theta^*})^{-1} [\delta(c_{\theta^*} - \hat{c}_{\theta^*}) + \delta(c_{\theta^*} + \hat{c}_{\theta^*})] \Theta \left[\omega - \frac{1}{2} (b_\theta c_\theta^2 + b_{\phi^*} c_{\phi^*}^2 + o(c_j^3)) \right] \quad (33)$$

in Eq. (29) and integrating over c_{θ^*} leads to the following threshold behavior for the cross section:

$$\begin{aligned} \left(\frac{d\sigma}{d(\Delta R)} \right)_{\text{threshold}} &\simeq \left[\frac{d\sigma(\bar{q}q \rightarrow W/Z\pi_T)}{dc_\theta} \right]_{c_\theta=c_{\theta^*}, c_{\phi^*}=0} B(\pi_T \rightarrow \bar{q}q) \\ &\times \frac{\sqrt{2}}{2\pi} \left(\frac{1}{b_{\theta^*}} \right)^{1/2} \int dc_\theta dc_{\phi^*} \frac{\Theta \left[\omega - \frac{1}{2} (b_\theta c_\theta^2 + b_{\phi^*} c_{\phi^*}^2 + \mathcal{O}(c^3)) \right]}{\left[\omega - \frac{1}{2} (b_\theta c_\theta^2 + b_{\phi^*} c_{\phi^*}^2 + \mathcal{O}(c^3)) \right]^{1/2}}. \end{aligned} \quad (34)$$

It is convenient to trade c_θ, c_{ϕ^*} for new variables ρ, κ :

$$\rho \cos \kappa = \sqrt{b_\theta/2} c_\theta, \quad \rho \sin \kappa = \sqrt{b_{\phi^*}/2} c_{\phi^*}, \quad (0 \leq \rho \leq \sqrt{\omega}, \quad 0 \leq \kappa < 2\pi). \quad (35)$$

The integral in Eq. (34) then yields our final result, the square-root behavior of $d\sigma/d(\Delta R)$ at threshold:

$$\left(\frac{d\sigma}{d(\Delta R)} \right)_{\text{threshold}} \simeq 2^{3/2} \sqrt{\frac{\Delta R - (\Delta\chi)_{\min}}{b_\theta b_{\theta^*} b_{\phi^*}}} \left[\frac{d\sigma(\bar{q}q \rightarrow W/Z\pi_T)}{dc_\theta} \right]_0 B(\pi_T \rightarrow \bar{q}q). \quad (36)$$

References

- [1] **CDF** Collaboration, T. Aaltonen *et. al.*, “Invariant Mass Distribution of Jet Pairs Produced in Association with a W boson in ppbar Collisions at $\sqrt{s} = 1.96$ TeV,” *Phys. Rev. Lett.* **106** (2011) 171801, 1104.0699.
- [2] **CDF** Collaboration http://www-cdf.fnal.gov/physics/ewk/2011/wjj/7_3.html.
- [3] **D0** Collaboration, V. M. Abazov, “Bounds on an anomalous dijet resonance in W+jets production in ppbar collisions at $\sqrt{s} = 1.96$ TeV,” *Phys. Rev. Lett.* **107** (2011) 011804, 1106.1921.
- [4] A. Annovi, “Physics Beyond the Standard Model, talk at Lepton-Photon 2011, Mumbai, India.” 2011.
- [5] E. J. Eichten, K. Lane, and A. Martin, “Technicolor at the Tevatron,” *Phys. Rev. Lett.* **106** (2011) 251803, 1104.0976.
- [6] E. Eichten, K. Lane, and A. Martin, “Testing CDF’s Dijet Excess and Technicolor at the LHC,” 1107.4075.
- [7] B. Holdom, “Raising the sideways scale,” *Phys. Rev.* **D24** (1981) 1441.
- [8] T. W. Appelquist, D. Karabali, and L. C. R. Wijewardhana, “Chiral hierarchies and the flavor changing neutral current problem in technicolor,” *Phys. Rev. Lett.* **57** (1986) 957.
- [9] K. Yamawaki, M. Bando, and K.-i. Matumoto, “Scale invariant technicolor model and a technidilaton,” *Phys. Rev. Lett.* **56** (1986) 1335.
- [10] T. Akiba and T. Yanagida, “Hierarchic chiral condensate,” *Phys. Lett.* **B169** (1986) 432.
- [11] E. Eichten and K. D. Lane, “Dynamical Breaking of Weak Interaction Symmetries,” *Phys. Lett.* **B90** (1980) 125–130.
- [12] K. D. Lane and E. Eichten, “Two Scale Technicolor,” *Phys. Lett.* **B222** (1989) 274.
- [13] **D0 Collaboration** Collaboration, V. Abazov *et. al.*, “Search for techniparticles in e+jets events at D0,” *Phys.Rev.Lett.* **98** (2007) 221801, hep-ex/0612013.
- [14] **CDF Collaboration** Collaboration, T. Aaltonen *et. al.*, “Search for Technicolor Particles Produced in Association with a W Boson at CDF,” *Phys.Rev.Lett.* **104** (2010) 111802, 0912.2059.
- [15] K. Lane and A. Martin, “An Effective Lagrangian for Low-Scale Technicolor,” *Phys. Rev.* **D80** (2009) 115001, 0907.3737.

- [16] K. Lane and S. Mrenna, “The collider phenomenology of technihadrons in the technicolor Straw Man Model,” *Phys. Rev.* **D67** (2003) 115011, hep-ph/0210299.
- [17] E. Eichten and K. Lane, “Low-scale technicolor at the Tevatron and LHC,” *Phys.Lett.* **B669** (2008) 235–238, 0706.2339.
- [18] G. Brooijmans *et. al.*, “New Physics at the LHC: A Les Houches Report. Physics at Tev Colliders 2007 – New Physics Working Group,” 0802.3715.
- [19] G. Brooijmans *et. al.*, “New Physics at the LHC. A Les Houches Report: Physics at TeV Colliders 2009 - New Physics Working Group,” 1005.1229.
- [20] T. Sjostrand, S. Mrenna, and P. Skands, “PYTHIA 6.4 physics and manual,” *JHEP* **05** (2006) 026, hep-ph/0603175.
- [21] C. Kilic and S. Thomas, “Signatures of Resonant Super-Partner Production with Charged-Current Decays,” *Phys. Rev.* **D84** (2011) 055012, 1104.1002.
- [22] Q.-H. Cao *et. al.*, “W plus two jets from a quasi-inert Higgs doublet,” *JHEP* **08** (2011) 002, 1104.4776.
- [23] C.-H. Chen, C.-W. Chiang, T. Nomura, and Y. Fusheng, “A light charged Higgs boson in two-Higgs doublet model for CDF Wjj anomaly,” 1105.2870.
- [24] J. Fan, D. Krohn, P. Langacker, and I. Yavin, “A Higgsophilic s-channel Z' and the CDF $W+2J$ Anomaly,” *Phys. Rev.* **D84** (2011) 105012, 1106.1682.
- [25] D. K. Ghosh, M. Maity, and S. Roy, “R parity violating supersymmetric explanation for the CDF Wjj excess,” *Phys. Rev.* **D84** (2011) 035022, 1107.0649.
- [26] J. F. Gunion, “A two-Higgs-doublet interpretation of a small Tevatron Wjj excess,” 1106.3308.
- [27] M. R. Buckley, D. Hooper, J. Kopp, and E. Neil, “Light Z' Bosons at the Tevatron,” *Phys. Rev.* **D83** (2011) 115013, 1103.6035.
- [28] J. Hewett and T. Rizzo, “Dissecting the Wjj Anomaly: Diagnostic Tests of a Leptophobic Z' ,” 1106.0294v1.
- [29] R. Harnik, G. D. Kribs, and A. Martin, “Quirks at the Tevatron and Beyond,” *Phys. Rev.* **D84** (2011) 035029, 1106.2569.
- [30] B. A. Dobrescu and G. Z. Krnjaic, “Weak-triplet, color-octet scalars and the CDF dijet excess,” 1104.2893v1.
- [31] A. E. Nelson, T. Okui, and T. S. Roy, “A unified, flavor symmetric explanation for the t-tbar asymmetry and Wjj excess at CDF,” *Phys. Rev.* **D84** (2011) 094007, 1104.2030.

- [32] F. Yu, “A Z' Model for the CDF Dijet Anomaly,” *Phys. Rev.* **D83** (2011) 094028, 1104.0243.
- [33] K. Cheung and J. Song, “Baryonic Z' Explanation for the CDF W_{jj} Excess,” *Phys. Rev. Lett.* **106** (2011) 211803, 1104.1375.
- [34] E. Eichten, K. D. Lane, and J. Womersley, “Finding low scale technicolor at hadron colliders,” *Phys.Lett.* **B405** (1997) 305–311, hep-ph/9704455.
- [35] **ATLAS** Collaboration, “Invariant mass distribution of jet pairs produced in association with a leptonically decaying W boson using 1.02 fb^{-1} of ATLAS data.” ATLAS-CONF-2011-097.
- [36] M. L. Mangano, M. Moretti, F. Piccinini, R. Pittau, and A. D. Polosa, “ALPGEN, a generator for hard multiparton processes in hadronic collisions,” *JHEP* **07** (2003) 001, hep-ph/0206293.
- [37] M. Mangano <http://mlm.web.cern.ch/mlm/talks/lund-alpgen.pdf>, 2004.
- [38] J. M. Campbell, R. K. Ellis, and C. Williams, “Vector boson pair production at the LHC,” *JHEP* **07** (2011) 018, 1105.0020.
- [39] M. Cacciari and G. P. Salam, “Dispelling the N^3 myth for the k_t jet-finder,” *Phys. Lett.* **B641** (2006) 57–61, hep-ph/0512210.
- [40] **D0** Collaboration, V. M. Abazov *et. al.*, “Search for a resonance decaying into WZ boson pairs in $p\bar{p}$ collisions,” *Phys. Rev. Lett.* **104** (2010) 061801, 0912.0715.
- [41] **CMS** Collaboration, “Search for the W' (or techn-rho) to WZ.” CMS PAS EXO-11-041.